



## Nanostructural, Optical and Electrical Properties of Al Doped TiO<sub>2</sub> Synthesized by Solid State Diffusion Method

Aung Than Htwe\*, Soe Maung, Maung Htwe and Myint Naing Tun

Department of Chemistry, University of Yangon, Yangon, Myanmar

### ABSTRACT

In this work, the three aluminium doped TiO<sub>2</sub> nanoparticles (AlTi-1, AlTi-2 and AlTi-3) of general formula of Al<sub>x</sub>Ti<sub>1-x</sub>O<sub>2</sub> (0.03 ≤ x ≤ 0.05) have been successfully synthesized by solid state diffusion method. The three Al doped TiO<sub>2</sub> nanoparticle obtained were sintered at 800°C for 8 h. The prepared particles were characterized by standard analytical techniques such as X-ray Diffraction (XRD), Scanning Electron Microscopy (SEM) and EDS equipment, Fourier Transform Infrared Spectroscopy (FT IR), Thermogravimetric Differential Analysis (TG DTA). Optical and dielectric studies have been investigated by Ultraviolet (UV-Visible) absorption spectroscopy and Impedance spectroscopy (LCR) meter respectively. XRD and SEM results confirmed the formation of nanoparticles with polycrystalline single phase nature with tetragonal anatase structure. It is found that crystalline size decreased with Al content. FT IR analysis was carried out to recognize the chemical bonds present in the system. FT IR spectroscopic analyses showed strong Ti-O-Ti and Al-O bonding. The optical properties were determined by UV-Visible spectroscopy in the wavelength range 200 nm-800 nm. The energy band gap values using Tauc's plot were found to be about 2.6 eV, 3.1 eV, 3.2 eV and 3.1 eV for pure TiO<sub>2</sub>, AlTi-1, AlTi-2 and AlTi-3 samples. Its results showed that optical band increases when Al is doped into pure TiO<sub>2</sub> sample. Frequency dependence of dielectric behaviour of the prepared samples was examined by LCR meter in the frequency range of 100 kHz-1000 kHz. The ac analysis showed that the dielectric constant (ε) and dielectric loss (tan δ) decrease with the increase in frequency. The dielectric property decrease with the increase in dopant concentration.

**Keywords:** Al doped TiO<sub>2</sub>; Solid state diffusion; Optical properties; Electrical properties

### INTRODUCTION

Titanium oxide (TiO<sub>2</sub>) is a dielectric material having energy band gap (E<sub>g</sub>=3.2 eV at 27°C). There exist three main structural phases: Rutile (tetragonal), anatase (tetragonal) and brookite (orthorhombic). TiO<sub>2</sub> has become one of the most important semiconductor materials in daily life, moreover, it has been widely used in fuel cell, solar energy conversion, photocatalysts/catalyst for environmental remediation processes, white pigment in paints and paper, bone implant material, Ultra-Violet (UV) absorber in sunscreen cream and other cosmetic

products, and additive in food products. Titanium dioxide, in comparison with other semiconductor catalysts, has many advantages such as suitable optical and electron properties, chemical stability, corrosion resistance, and non-toxicity, making it a perfect candidate for photocatalytic processes. However, the development of TiO<sub>2</sub> as a material in electronic device applications has often been hindered by its high electrical resistivity. A popular solution for this is to dope it with other elements to increase the electron density, thus lowering the electrical resistivity [1].

<b>Received:</b>	25-August-2020	<b>Manuscript No:</b>	IPNNR-20-5928
<b>Editor assigned:</b>	28-August-2020	<b>PreQC No:</b>	IPNNR-20-5928 (PQ)
<b>Reviewed:</b>	11-September-2020	<b>QC No:</b>	IPNNR-5928
<b>Revised:</b>	09-November-2022	<b>QI No:</b>	IPNNR-20-5928
		<b>Manuscript No:</b>	IPNNR-20-5928 (R)
<b>Published:</b>	07-December-2022	<b>DOI:</b>	10.12769/ipnnr-22.6.39

**Corresponding author** Aung Than Htwe, Department of Chemistry, University of Yangon, Myanmar, Tel: 9957309102; E-mail: aungthanhtwe76@gmail.com

**Citation** Than HA, Maung S, Htwe M, Tun MN (2022) Nanostructural, Optical and Electrical Properties of Al Doped TiO<sub>2</sub> Synthesized by Solid State Diffusion Method. J Nanosci Nanotechnol Res. 6:39.

**Copyright** © Than HA, et al. This is an open-access article distributed under the terms of the Creative Commons Attribution License, which permits unrestricted use, distribution, and reproduction in any medium, provided the original author and source are credited.

Doping and/or deposition are effective strategies to increase spectral response of TiO<sub>2</sub> through narrowing electronic properties and by altering optical responses. The metal ions deposited on the TiO<sub>2</sub> surface usually act as a sink for the photo-induced charge carriers and thus can improve the interfacial charge transfer processes. The materials have been under investigation for TiO<sub>2</sub> doping/depositions are noble metals such as (Pt, Au, Pd, Rh, Ni, Cu, Sn, Ag), transition metals such as (Zn, Fe, Mn, Co, Pd, Ni, etc.), rare-earth metals such as (La, Ce, Pr, Nd, Sm, Eu, Dy, Gd), other metals and non-metal ions. Aluminium (Al) is one of the elements used as dopant for TiO<sub>2</sub>. Successful Al doping of TiO<sub>2</sub> has been reported using simultaneous radio frequency and dc magnetron sputtering, dc plasma jet, auto combustion and pulsed laser deposition method. However, there are still not many comprehensive studies on Al doping of TiO<sub>2</sub> using the solution method. Prepared Al-doped TiO<sub>2</sub> nanoparticles using a citrate-nitrate autocombustion system with Ti solution and Al(NO<sub>3</sub>)<sub>3</sub> solution as precursors. Prepared Al-doped TiO<sub>2</sub> ceramic nanoparticles by a single-step direct combination of vaporized Ti, Al and O<sub>2</sub>, and these nanoparticles exhibited visible-light photocatalytic activity [2]. In this research work consists in the aluminium doped TiO<sub>2</sub> nanoparticles were obtained by sintering of the mixed powders at 800°C. Solid state diffusion method was also used to prepare the aluminium doped TiO<sub>2</sub> nanoparticles. The characteristics of prepared samples were investigated by XRD, SEM and FT IR analysis. Finally, the optical and electrical properties of prepared aluminium doped TiO<sub>2</sub> nanoparticles were determined by UV-visible spectrophotometer and LCR meter.

## MATERIALS AND METHODS

AR grade chemicals were used in this study without further purification. Aluminium nitrate (Al(NO<sub>3</sub>)<sub>3</sub>·9H<sub>2</sub>O) and Titanium Dioxide (TiO<sub>2</sub>) were used as starting chemicals. First, 0.2 M Al(NO<sub>3</sub>)<sub>3</sub>·9H<sub>2</sub>O was added to 1 M TiO<sub>2</sub> under constant magnetic stirring using an organic media (i.e., methanol). This mixture was maintained at room temperature overnight for complete removal of the methanol. The as-obtained product was sintered at 800°C [3].

### Preparation of the Al<sub>x</sub>Ti<sub>1-x</sub>O<sub>2</sub> (0.03 ≤ x ≤ 0.05) Nanoparticles

The three different Al-doped TiO<sub>2</sub> nanoparticles (Al<sub>0.03</sub>Ti<sub>0.97</sub>O<sub>2</sub> (AlTi-1), Al<sub>0.04</sub>Ti<sub>0.96</sub>O<sub>2</sub> (AlTi-2) and Al<sub>0.05</sub>Ti<sub>0.95</sub>O<sub>2</sub> (AlTi-3)) were prepared by a solid state diffusion route. Firstly the starting chemicals Al(NO<sub>3</sub>)<sub>3</sub>·9H<sub>2</sub>O was mixed directly with TiO<sub>2</sub> using an agate mortar and pestle at 24 hours. The crushed sample was calcined at 400°C for 2 hours and crushed again in mortar and pestle. The prepared samples were sintered at 800°C under Muffle Furnace for 8 hours. Finally, the sample in the crucible was allowed to cool at room temperature [4].

### Characterization of Materials

The microstructural analysis of the prepared samples of pure and Al doped TiO<sub>2</sub> were characterized for crystalline phase identification by XRD, SEM and EDS equipment. The chemical bonding and functional group information of pure and Al doped TiO<sub>2</sub> nanoparticles were analysed by FT IR spectroscopy in the wavenumber range of 400 cm<sup>-1</sup>-1000 cm<sup>-1</sup>. The UV-Visible spectra of pure and Al doped TiO<sub>2</sub> nanopowder were performed in

the range 200 nm-800 nm using Perkin Elmer spectrophotometer [5]. Dielectric properties were carried out in the frequency range of 100 kHz to 1 MHz using LCR meter (LCR-8110G meter).

## RESULTS

### X-ray Diffraction Analysis

The XRD pattern of TiO<sub>2</sub> and the Al-doped TiO<sub>2</sub> nanoparticles are synthesized by the solid-state diffusion routes. The position of the diffraction peaks in the pattern and the relative intensity data are in agreement with ICDD File card no. 01-84-1285 for anatase TiO<sub>2</sub>. The characteristics peaks of the Al-doped TiO<sub>2</sub> system are indicated in a symbolic manner. The XRD patterns of the Al-doped TiO<sub>2</sub> nanoparticles synthesized by the solid-state diffusion routes are also in excellent agreement with the parent TiO<sub>2</sub> with the characteristics peaks of aluminium [6]. Some characteristics peaks of aluminium were suppressed, which indicates that Al is nicely doped in the TiO<sub>2</sub> structure. These peaks corresponding to aluminium were indexed to ICDD card no. 01-081-1667. X-ray diffractogram of pure TiO<sub>2</sub> showed the major diffraction peaks at Miller indices of (101), (103), (004), (112), (200), (105), (211), (213), (204), (116) and (220). In AlTi-1 NPs showed the major diffraction peaks at Miller indices of (101), (103), (104), (112), (200), (105), (211), (213), (204), (116) and (220). In AlTi-2 NPs, additional nine diffraction peaks corresponding to (101), (103), (004), (112), (111), (200), (105), (211), (213), (204) and (116) planes were observed and assigned to the Al<sub>2</sub>O<sub>3</sub>. The X-ray diffractogram of AlTi-3 NPs showed nine diffraction peaks of (101), (103), (004), (112), (200), (105), (211), (213), (204) and (116) planes were observed and assigned to the Al<sub>2</sub>O<sub>3</sub>. The size of the Al doped TiO<sub>2</sub> nanoparticles prepared by the chemical route are smaller than the particles synthesized by the solid-state diffusion route. This increase in the particle size in the solid-state diffusion route is due to the annealing temperature because the increase in temperature may result in merging of the particles. Because the Al-doped TiO<sub>2</sub> belongs to the tetragonal system, the lattice constants are computed the following equation:

$$\frac{1}{d^2} = \frac{h^2 + k^2}{a^2} + \frac{l^2}{c^2}$$

where, a and c are the lattice constants and d is the lattice spacing. In comparison to anatase TiO<sub>2</sub>, the doping of Al into TiO<sub>2</sub> results in an increased in the a lattice parameter and a decrease in the c lattice parameter. This change in the lattice parameters results in a decrease in the particle size with increasing Al concentration [7]. The lattice parameters estimated for the Al-doped TiO<sub>2</sub> system synthesized by solid state diffusion are summarized in Table 1.

**Table 1:** Variable of crystallite size, lattice parameter and band gap and crystal structure with pure and Al doped TiO<sub>2</sub>.

Sample	Crystallite size (nm)	Band gap (eV)	Lattice parameter (Å)		Crystal structure
			a=b	c	
Pure TiO <sub>2</sub>	66.8	3	3.38	9.5	Tetragonal
AlTi-1	62.77	3.2	3.85	9.51	Tetragonal
AlTi-2	66.41	3.1	3.83	9.5	Tetragonal
AlTi-3	55.55	3.1	3.84	9.52	Tetragonal

Using Scherrer's equation, the average crystallite sizes were

determined to be 51.18 nm for pure  $\text{TiO}_2$ , 49.96 nm for AlTi-1, 51.83 nm for AlTi-2 and 46.54 nm for AlTi-3 for the material prepared by solid-state diffusion routes, respectively. This decrease in the size for the particles prepared by the solid state diffusion may be due to a lower annealing temperature and an increase in the lattice parameter (Figures 1-4).

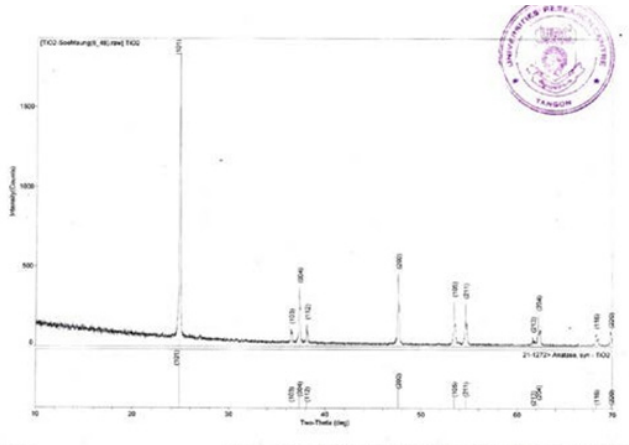


Figure 1: Figure 1 XRD pattern of pure  $\text{TiO}_2$  powder.

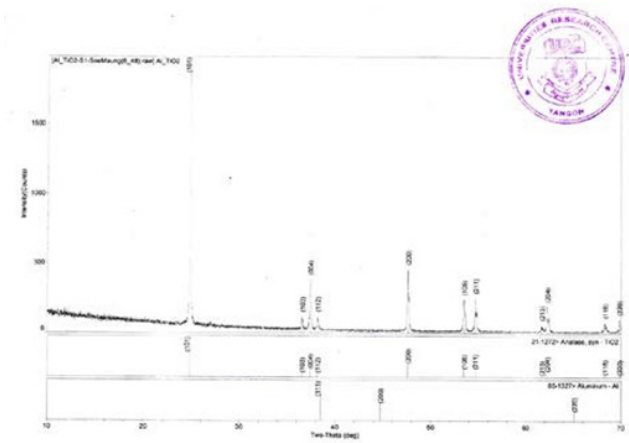


Figure 2: XRD pattern of prepared AlTi-1 powder at sintered temperature 800°C for 8 hours.

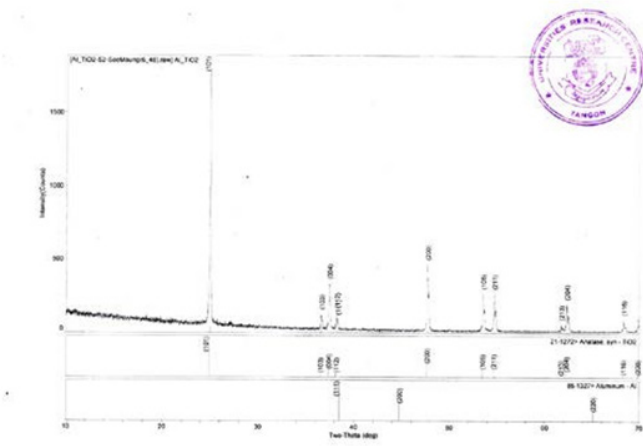


Figure 3: XRD pattern of prepared AlTi-2 powder at sintered temperature 800°C for 8 hours.

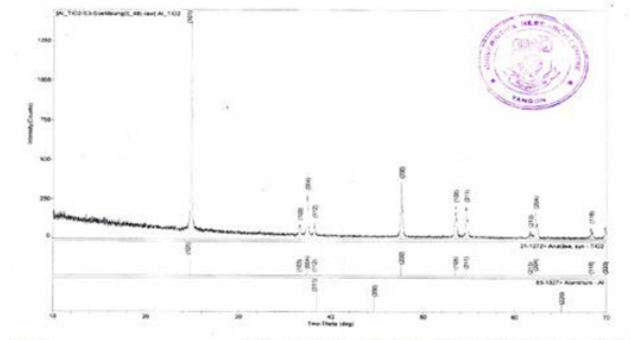


Figure 4: XRD pattern of prepared AlTi-3 powder at sintered temperature 800°C for 8 hours.

The crystallite size of  $\text{TiO}_2$  decreases from about 66.80 nm to 55.55 nm when Al content increases from 0% to 0.05%. The data shows that the presence of Al ions in  $\text{TiO}_2$  allows the growth of crystal grains and slow the motion of a grain boundary.

### SEM and EDS Analysis

The surface morphology and the composition of the pure  $\text{TiO}_2$ , doped sample of AlTi-1, AlTi-2 and AlTi-3 have been investigated using SEM and the result for these four samples are displayed in Figure 5. All figures are obtained at 5 kV and 15 kV accelerating voltage respectively [8]. It can be clearly seen that the nanostructure of the particles is completely different. It can be seen in figure that all the samples show a particle like structure with particle size of 100 nm. These nanoparticles appear to be porous, and the porosity increases with increasing aluminium doping concentration. They are also evident from the analysis of SEM image that. The particles form a cluster of nanocrystalline  $\text{TiO}_2$  due to agglomeration. The semi quantification of elemental analyses to identify the weight percentage of major and minor elements present in the samples were done using Energy Dispersive X-ray Spectrometer (EDS), JEOL model, JSD-5610 LV with an accelerating voltage of 20 KV. The result of EDS analysis of pure  $\text{TiO}_2$ , AlTi-1, AlTi-2 and AlTi-3 sample are shown in Figure 6.

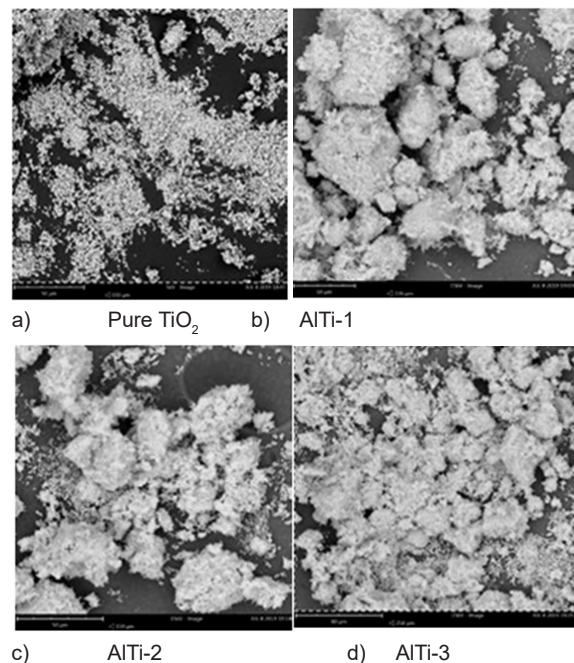
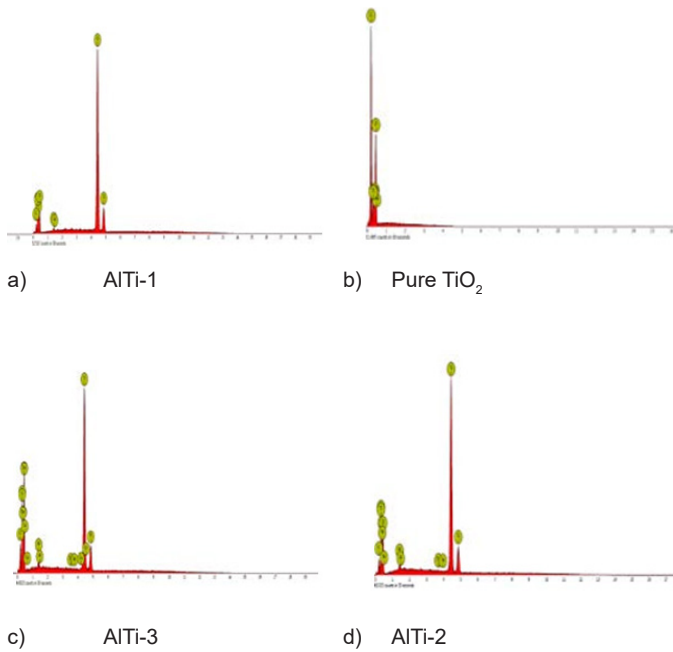


Figure 5: SEM micrograph of pure  $\text{TiO}_2$  and Al-doped  $\text{TiO}_2$  nanoparticles.



**Figure 6:** EDS analysis of pure and Al doped  $\text{TiO}_2$  nanoparticles illustrating the presence of constituents.

From quantitative analysis it is evident that contain approximately 33.01% Ti and 27.79% O by weight in pure  $\text{TiO}_2$ , 64.12% Ti, 0.42% Al and 30.98% O by weight in AlTi-1, 56.72% Ti, 1.22% Al and 35.38% O by weight in AlTi-2 and 40.27% Ti, 1.27% Al and 49.38% O by weight in AlTi-3 which confirms the dopant level in the sample. These results were further found consistent with the XRD data [9].

### FT IR Analysis

The Fourier Transform Infrared (FT IR) Spectra of pure  $\text{TiO}_2$ , AlTi-1, AlTi-2 and AlTi-3 nanoparticles were recorded in the range of  $4000\text{ cm}^{-1}$ - $400\text{ cm}^{-1}$  using UATR technique Perkin Elmer spectrometer. The recorded FT IR spectrum of pure  $\text{TiO}_2$  and Al doped  $\text{TiO}_2$  are shown in Figures 7-10. The different bonds and functional groups absorbed at different wavelengths, an infrared spectrum is used to determine the structure of organic molecules. Although this radiation is weak, it does supply sufficient energy for bonds in the molecule to vibrate by Stretching or Bending. The area from  $3500\text{ cm}^{-1}$  to  $1300\text{ cm}^{-1}$  is called the functional group region. The bands in this region are particularly useful in determining the type of functional groups present in the molecule. The area from  $1300\text{ cm}^{-1}$  to  $667\text{ cm}^{-1}$  is called the fingerprint region [10]. A peak-by-peak match of an unknown spectrum with the spectrum of the suspected compound in this region can be used, much like a fingerprint, to conform its identity. The reaction between precursor materials of various oxide doped  $\text{TiO}_2$  nanopowders are prepared by solid state diffusion method. The absorption band was observed in the range  $1000\text{ cm}^{-1}$ - $400\text{ cm}^{-1}$  for aluminium doped  $\text{TiO}_2$  nanoparticles. In the spectrum of pure  $\text{TiO}_2$ , the peak at  $419\text{ cm}^{-1}$  should be attributed to Ti-O bond in the  $\text{TiO}_2$  lattice (anatase titanium). For aluminium doped  $\text{TiO}_2$  nanoparticles and pure  $\text{TiO}_2$  nanoparticles, the peaks locked in the region  $431$  and  $407\text{ cm}^{-1}$  indicating the Ti-O-O band. According to data, the synthesized AlTi-1, AlTi-2 and AlTi-3 NPs agreement with the wavelength.

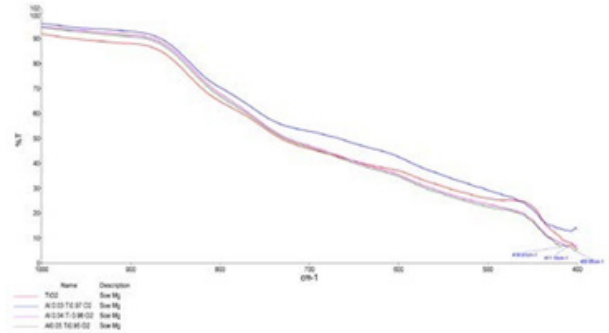


**Figure 7:** FT IR spectrum of pure and Al doped  $\text{TiO}_2$  nanoparticles.

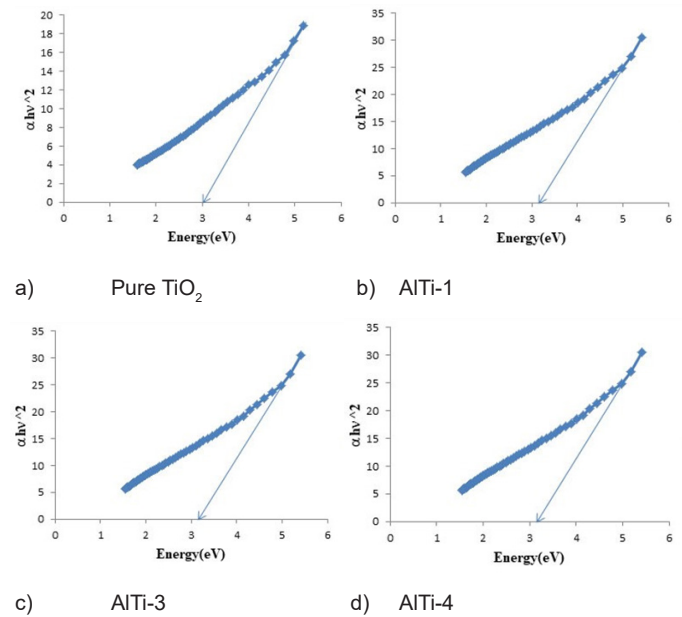


**Figure 8:** Plot of  $(ah\nu)^2$  Vs photon energy of pure and Al doped  $\text{TiO}_2$  nanoparticles.

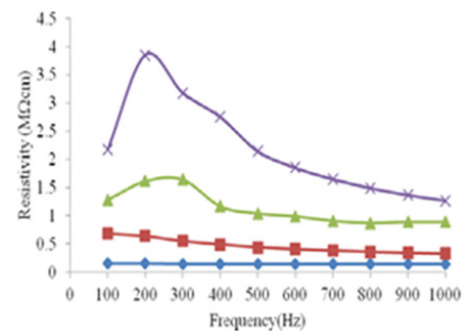


**Figure 9:** Variations of resistivity of pure  $\text{TiO}_2$  and Al doped  $\text{TiO}_2$  as a function of frequency. **Note:** ( $\bullet$ ) Pure  $\text{TiO}_2$ , ( $\blacksquare$ ) AlTi-1, ( $\blacktriangle$ ) AlTi-2, ( $\blacklozenge$ ) AlTi-3

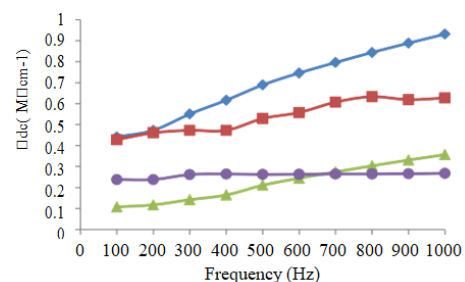


**Figure 10:** Variations of DC conductivity of pure  $\text{TiO}_2$  and Al doped  $\text{TiO}_2$  as a function of frequency. **Note:** ( $\bullet$ ) Pure  $\text{TiO}_2$ , ( $\blacksquare$ ) AlTi-1.

## Optical Properties

The photo-activity of titanium dioxide is depended on the band gap, the band gap of titanium dioxide lies in the UV range (3 eV for Rutile and 3.2 eV for Anatase), which takes a small fraction in the solar spectrum. The titanium dioxide could be doped either with noble metal such as gold, silver, platinum, or with non-metal materials such as nitrogen, fluorine, to improve the photo-activity [11]. The photoelectronic properties of semiconductor nanoparticles can be studied by using UV-Visible absorption spectroscopy (UV-Vis). The absorbance generally depends on several factors such as oxygen deficiency, band gap, impurity centers and surface roughness. The optical band gap of the nanopowders was calculated using the classical Tauc relationship as

$$\alpha h\nu = A(h\nu - E_g)^n$$

where the value of  $n=1/2, 3/2, 2$  or  $3$  depending on the nature of the electronic transition responsible for absorption Here  $n=2$  is used for indirect band gap semiconductor,  $\alpha$  is absorption coefficient,  $h$  is Planck's constant and  $\nu$  is the photo frequency. The indirect band gap value reported corresponding to  $n=2$  in literature for bulk anastases is estimated from 3.10 eV to 3.20 eV. An extrapolation of the linear region of a plot of  $h\nu$  versus  $(\alpha h\nu)^2$  gives the value of the optical band gap  $E_g$ . According to the band gap values, the Al doped  $\text{TiO}_2$  samples found within the semiconductor band-gap range. This conclusion based on the UV-Vis results is consistent with the previous XRD and SEM analyses (Figures 11-13).

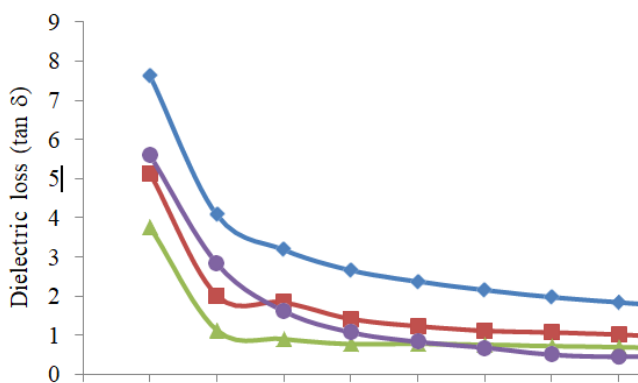


**Figure 11:** Variations of DC conductivity of pure  $\text{TiO}_2$  and Al doped  $\text{TiO}_2$  as a function of frequency. **Note:** (—♦—) Pure  $\text{TiO}_2$ , (—■—) AITi-1, (—▲—) AITi-2, (—●—) AITi-3

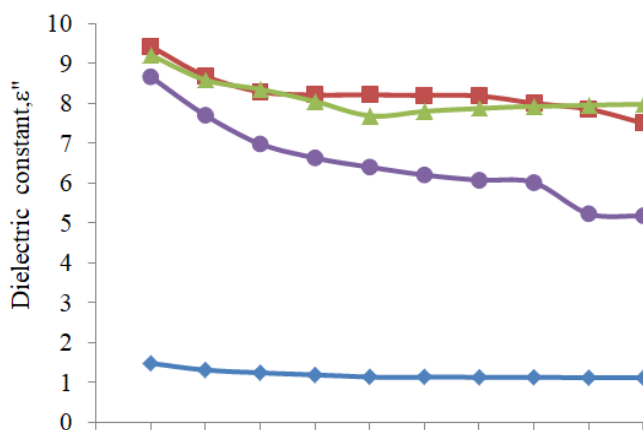


**Figure 12:** Variations of dielectric constant of pure  $\text{TiO}_2$  and Al doped  $\text{TiO}_2$  samples as a function of frequency. **Note:** (—♦—) Pure  $\text{TiO}_2$ , (—■—) AITi-1, (—▲—) AITi-2, (—●—) AITi-3

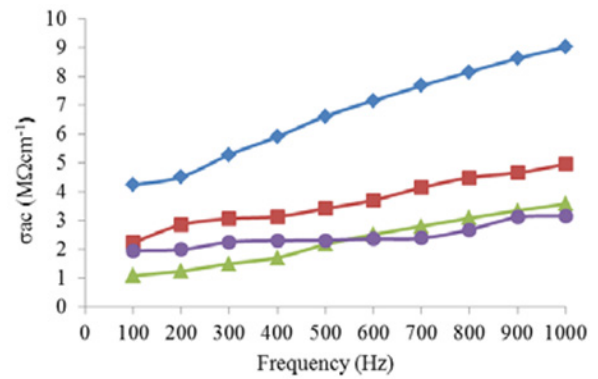


**Figure 13:** Variations of AC conductivity pure  $\text{TiO}_2$  and Al doped  $\text{TiO}_2$  as a function of frequency. **Note:** (—♦—) Pure  $\text{TiO}_2$ , (—■—) AITi-1, (—▲—) AITi-2, (—●—) AITi-3

## Electrical Properties

The electrical properties of the pure  $\text{TiO}_2$  and Al doped  $\text{TiO}_2$  nanoparticle samples were carried out by using LCR (Inductance, capacitance and resistance) meter. Dielectric analysis measures the electrical properties of a material as a function of frequency. The conductivity and dielectric parameter of pure  $\text{TiO}_2$  and Al doped  $\text{TiO}_2$  nanoparticles have been investigated in the frequency range of 100 kHz-1000 kHz. There are two forms of electrical conductivity, frequency independent DC conductivity and frequency dependent AC conductivity upon increasing the frequency [12]. The experimental results indicate that AC conductivity, dielectric constant and dielectric loss depend on the frequency. The AC conductivity was derived from dielectric constant and dielectric loss data.

## Variations of Resistivity and DC Conductivity

The electrical resistivity of a conductor material is a measure of how strongly the material opposes the flow of electric current through it. The resistivity factor enables the resistance of different types of conductors at a specified temperature according to their physical properties without regards to their lengths or the cross sectional area. The dc conductivity is determined only by resistance. The electrical resistance of a conductor is directly proportional to its length and inversely proportional to its cross-sectional area. The conductivity is the reciprocal of the resistivity [13]. Therefore, the higher value of resistivity has the lower value of dc conductivity. It was found that the resistivity value of pure  $\text{TiO}_2$ , AITi-1, AITi-2 and AITi-3 prepared slightly decrease with increase in frequency. The higher resistivity observes for doped samples AITi-1, AITi-2 and AITi-3 prepared than pure  $\text{TiO}_2$ . On the other hand, the lower conductivity value of doped samples AITi-1, AITi-2 and AITi-3 found in (Figure 14).

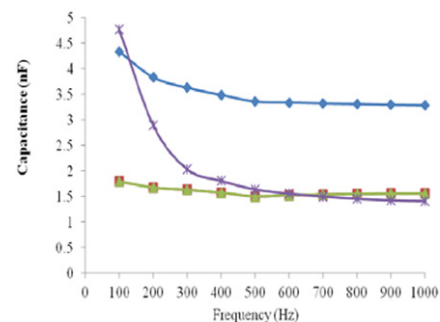


**Figure 14:** Variations of capacitance of pure  $\text{TiO}_2$  and Al doped  $\text{TiO}_2$  as a function of frequency. **Note:** (—♦—) Pure  $\text{TiO}_2$ , (—■—) AITi-1, (—▲—) AITi-2, (—●—) AITi-3

## Variations of Dielectric loss, Dielectric constant and AC conductivity

Dielectric analysis studied the electrical properties of a material as a function of frequency and measures the two fundamental electrical characteristic of materials. The first one is the capacitive nature, which represents its ability to store electric charge. The other is the conductive nature which represents its ability to transfer electronic charge. Through the analysis, the dielectric loss and dielectric constant of a material can be determined. Loss tangent or loss factor  $\tan \delta$  represents the energy dissipation in the dielectric system. The variation of dielectric loss of pure  $\text{TiO}_2$ , AlTi-1, AlTi-2 and AlTi-3 with frequency range from 100 kHz to 1000 kHz. The dielectric loss arises due to the impurities and defects in the crystal lattice when the polarization lags behind the applied alternating field. It was found from the plots that  $\tan \delta$  (loss) decreases with the increase in frequency for all of the samples. At low frequencies dielectric losses are large due to space charge polarization. The space charge polarization arises due to inhomogeneous dielectric structure. The inhomogeneity present in the system is in the form of porosity and grain structure. High porosity and low density results in low dielectric constant and dielectric losses. At higher frequency the losses are found to be small since domain wall motion is withdrawn and magnetization is forced to alteration of dipolar rotation. It is found that the overall values of  $\tan \delta$  are found to decrease with increasing the concentration of Al ions for all the samples. It can be seen from these table and figures that the dielectric constant decreases with the increase in frequency and becomes almost independent of frequency in high frequency region. It was found that the dielectric loss and dielectric constant decrease with increase in frequency [14]. When the frequency is increased, the orientation polarization decrease since it takes more time than electronic and ionic polarization. The ac conductivity of pure  $\text{TiO}_2$ , AlTi-1, AlTi-2 and AlTi-3 prepared increase linearly with increasing frequency. The value of ac conductivity increase at higher frequency 1000 kHz (1MHz) is caused due to oxygen ion vacancy. It shows that the ac conductivity of AlTi-1, AlTi-2 and AlTi-3 is greater than pure  $\text{TiO}_2$ .

## Variations of capacitance

Capacitance techniques monitor the movement of electronic charge within a semiconductor device and provide a measure of free-carrier and electrically active defect-state properties. Capacitance is the charge storage capacity and is measured across a rectifying junction. The frequency dependence capacitance of pure  $\text{TiO}_2$  and AlTi-1, AlTi-2 and AlTi-3 samples was measured within the frequency range of 100 kHz to 1000 kHz at room temperature. The capacitance of pure  $\text{TiO}_2$  and AlTi-1, AlTi-2 and AlTi-3 samples are high at low frequency region due to contribution of all kinds of polarization at low frequency, then decrease with increase of frequency and finally approaches to all most constant value above 600 kHz. This is due to the change of space charge, ionic and orientation polarization at higher frequency. It is found that the capacitance value of AlTi-3 samples is greater than pure  $\text{TiO}_2$ , AlTi-1 and AlTi-2. The dielectric constant was calculated from the measured capacitance obtain by LCR meter pure  $\text{TiO}_2$  and AlTi-1, AlTi-2 and AlTi-3 exhibit capacitance of average  $10^{-9} \sim 10^{-11}$  F. Thus the range

of capacitance probably belonged to grain boundary [15]. The highest capacitance value is obtained which gives 4.3 nF for pure  $\text{TiO}_2$ , 1.516 nF for AlTi-1, 1.8026 nF for AlTi-2 and 47.734 pF for AlTi-3 at 100 kHz. The capacitance related to the ability of pure  $\text{TiO}_2$  and AlTi-1, AlTi-2 and AlTi-3 sample to collect and store energy in the form of an electrical charge.

## CONCLUSION

The pure and Al doped  $\text{TiO}_2$  nanoparticles were successfully prepared by solid state diffusion method. XRD spectra show that all of the prepared pure and Al doped  $\text{TiO}_2$  nanoparticles are tetragonal structure. The average crystalline size of pure  $\text{TiO}_2$ , AlTi-1, AlTi-2 and AlTi-3 NPs was 51.18 nm, 49.96 nm, 51.83 nm and 46.54 nm respectively. The SEM image of AlTi-1 and AlTi-3 revealed the agglomeration of the particles and that of AlTi-2 showed fluffy surface. The Ti-O bond of anatase phase in all the synthesized samples was identified by FT IR measurements. From FT IR spectral data of AlTi-1, AlTi-2 and AlTi-3, Metal-O bond was observed at  $410 \text{ cm}^{-1}$ ,  $411 \text{ cm}^{-1}$ ,  $419 \text{ cm}^{-1}$  and  $431 \text{ cm}^{-1}$ . In the spectrum of pure  $\text{TiO}_2$ , the peak at  $419 \text{ cm}^{-1}$  should be attributed to Ti-O bond in the  $\text{TiO}_2$  lattice (anatase titanium). The SEM analysis reveals that the morphology of Al doped  $\text{TiO}_2$  nanoparticles appear to be porous, and the porosity increases with increasing aluminium doping concentration. They are also evident from the analysis of SEM image that the particles form a cluster of nanocrystalline  $\text{TiO}_2$  due to agglomeration. Incorporation of Al was confirmed from elemental analysis using EDX. AlTi-3 sample is seen that the increasing Al doped occurs. The as-synthesized samples exhibit an intense absorption in the UV region at approximately 230 nm-240 nm, which indicates that this material exhibits quantum confinement. The UV-Visible shows Al doped titanium nanoparticles extend the absorption edge ultraviolet to visible range and make the green shift more distinct and also analyses the band gap value. The band gap values of  $\text{TiO}_2$ , AlTi-1, AlTi-2 and AlTi-3 are 3.0eV, 3.2eV, 3.1eV and 3.1eV respectively. These value are within the semiconductor band gap range and all agreed with literature. The electrical properties of the pure  $\text{TiO}_2$ , AlTi-1, AlTi-2 and AlTi-3 samples were also showed by LCR (Inductance, Capacitance and Resistance) meter in the frequency range of 100 kHz-1000 kHz. It was observed that the AC conductivity value of pure  $\text{TiO}_2$ , AlTi-1, AlTi-2 and AlTi-3 are  $4.24 \text{ M}\Omega\text{cm}^{-1}$ ,  $2.24 \text{ M}\Omega\text{cm}^{-1}$ ,  $1.09 \text{ M}\Omega\text{cm}^{-1}$  and  $1.96 \text{ M}\Omega\text{cm}^{-1}$ . It was found that undoped  $\text{TiO}_2$  is lower conductivity. The conductivity value of Al doped  $\text{TiO}_2$  are greater than that of undoped sample.

## ACKNOWLEDGEMENT

The author feel indebted to Professor and Head Dr. Ni Ni Than, Department of Chemistry, University of Yangon, Yangon, Myanmar, for his stimulating suggestions.

## REFERENCES

1. Ahmed Hara (2015) Preparation and characterization of copper-doped and silver-doped titanium dioxide nano-catalysts for photo catalytic applications.
2. Tsai C, H Hsi, H Bai, KS Fan, H Sun, et al. (2012) Single-step synthesis of al-doped  $\text{TiO}_2$  nanoparticles using non-transferred thermalplasma torch. J Appl Phys 51: 1-6.

3. Nemade KR, RV Barde, SA Waghuley (2016) Liquefied petroleum gas sensing by Al doped TiO<sub>2</sub> nanoparticles synthesized by chemical and solid-state diffusion routes. *J Taibah Univ Sci* 10: 345-351.
4. M Z Musa (2011) Aluminium doping of titanium dioxide thin films using sol-gel method. *J Res Sci Tech* 8: 21-28.
5. Tahir M, Amin NAS (2013) Advances in visible light responsive titanium oxide-based photocatalysts for CO<sub>2</sub> conversion to hydrocarbon fuels. *Energy Convers Manag* 76: 194-214.
6. Choig YJ, ZSeeley S, Bandyopadhyay A, Bose S (2007) Aluminium-doped TiO<sub>2</sub> nano-powders for gas sensors. *Sens Actu B* 124: 111-117.
7. Tsai CY, TH Kuo, HC His (2011) Fabrication of Al-doped TiO<sub>2</sub> visible-light photocatalyst for low concentration mercury removal. *Int J Photoene* 41: 63-69.
8. Bahadur J, S Agrawal, A Parveen, A Jawad, SSZ Ghalib, et al. (2015) Microstructural, optical and dielectric properties of Ag doped TiO<sub>2</sub> synthesized by Sol-gel method. *Mater Focus* 4: 134-141.
9. Muna Muzahim Abbas MR (2020). Solid state reaction synthesis and characterization of aluminum doped titanium dioxide nanomaterials. *J South West Jiaotong Univ* 55: 45-51.
10. Garzon Roman A, Zuñiga Islas C, Quiroga González E (2020) Immobilization of doped TiO<sub>2</sub> nanostructures with Cu or In inside of macroporous silicon using the solvothermal method: Morphological, structural, optical and functional properties. *Cera Intern* 46: 1137-1147.
11. Nemade KR, Barde RV, Waghuley SA (2016) Liquefied petroleum gas sensing by Al-doped TiO<sub>2</sub> nanoparticles synthesized by chemical and solid-state diffusion routes. *J Taibah Univ Sci* 10: 345-351.
12. Das K, Sharma SN, Kumar M, De SK (2009) Morphology dependent luminescence properties of Co doped TiO<sub>2</sub> nanostructures. *J Phys Chem C* 113: 14783-14792.
13. Pillai VV, Lonkar SP, Alhassan SM (2020) Template-free, solid-state synthesis of hierarchically macroporous S-doped TiO<sub>2</sub> nano-photocatalysts for efficient water remediation. *ACS Omega* 5: 7969-7978.
14. Schoonman J (2000) Nanostructured materials in solid state ionics. *Solid State Ionics* 135: 5-19.
15. Stride JA, Tuong NT (2010) Controlled synthesis of titanium dioxide nanostructures. *Solid State Phen* 162: 261-294.